Modeling Equivalent Radiation Sources for PCBs Using Dipole Approximation and Near-Field Scanning

Victor S. Chebanov
Department of Television and Control
Tomsk State University of Control
Systems and Radioelectronics (TUSUR)
Tomsk, Russia
viktor.s.chebanov@tusur.ru

Valerii A. Semeniuk
Department of Television and Control
Tomsk State University of Control
Systems and Radioelectronics (TUSUR)
Tomsk, Russia
valerii.a.semeniuk@tusur.ru

***Abstract*—Modern electronic design requires electromagnetic compatibility (EMC) to be efficiently assessed. While anechoic chamber testing is accurate, its high cost necessitates rapid emission prediction during prototyping. However, raw near-field scanning data lacks the versatility needed for full-system simulation. This study presents a novel methodology for constructing compact equivalent radiation source models by applying dipole approximation to near-field data. The algorithm extracts electric and magnetic dipole moments from tangential magnetic field components. By incorporating image theory and perfect electric conductor boundary conditions, we reduced the model. The methodology was validated on a microstrip line, a meander line, and an STM microcontroller. Experimental results confirmed high correlation between measured and reconstructed fields, with a maximum absolute deviation of 28 fA/m and average errors below 1%. The developed methodology allows experimental measurement results to be effectively transformed into mathematical models suitable for integration into Computer-Aided Design systems. This approach enables comprehensive EMC analysis of electronic equipment at early design stages, thus significantly reducing the volume of full-scale testing.**

Keywords—dipole moment, electromagnetic compatibility, equivalent radiation sources, near-field, printed circuit board, radiated emissions.

I. Introduction

Printed circuit board (PCB) design is a critical stage in the development of modern electronic equipment and requires comprehensive technical solutions to ensure electromagnetic compatibility (EMC). Traditionally, radiated emission levels of electronic equipment are assessed in anechoic or reverberation chambers, as well as using TEM cells [1], [2], [3]. While these methods provide high accuracy for finished products, they are labor-intensive and costly, especially during prototyping. In this respect, near-field surface scanning has emerged as a promising alternative, enabling rapid localization of electromagnetic radiation sources. However, directly interpreting scanning results is often insufficient for systemic EMC analysis, far-field recalculation [4], or integration into computer-aided design systems. Therefore, transforming the measured radiated emission levels is necessary, which can be achieved through various approaches.

According to the multipole expansion theory [5], any electrically small source can be represented by a set of elementary electric and magnetic dipoles. Such models have successfully been used for simulation [6], [7], [8], [9], and their parameters have been calculated based on near-field measurements [10], [11]. To solve the inverse problem of extracting these dipole moments from measured data, various approaches have been developed, ranging from classical analytical methods to genetic [12] and metaheuristic [13] algorithms. Several studies have used image processing to determine the number and initial positions of the dipoles [14]. Additionally, combining the analytical Green's function with continuous basis functions allowed achieving a resolution of less than half a wavelength while remaining robust against noise [15].

Moreover, numerical methods have effectively been applied to construct equivalent source models [16], [17]. The obtained equivalent sources can be integrated into computer-aided design systems [18], [19], for example, to analyze induced currents and voltages in transmission lines [20]. However, despite the multitude of existing methods, a comprehensive solution covering the setup assembly, data measurement, and dipole moment calculation is still lacking.

Thus, it is highly relevant to develop a methodology for converting measured radiated emission levels, which would include a setup for measuring the radiated emissions of a device under test (DUT). Accordingly, this paper aims to develop and validate a methodology for transforming measured near-field radiated emissions into equivalent dipole radiation sources.

II. Methodology for Equivalent Dipole Source Modeling

A. Between Dipole Moments and Radiated Emissions

In a Cartesian coordinate system, any arbitrary electrically small source can be replaced by six dipoles using the dipole approximation of the multipole expansion (representing the DUT electromagnetic radiation as a superposition of a set of elementary dipoles) [21]. Three of these dipoles are electric and three are magnetic; all are oriented along the *x*, *y*, and *z* axes (Fig. 1) and denoted as P_x, P_y, P_z and M_x, M_y, M_z respectively [5]. The superposition of electromagnetic fields generated by the set of dipole moments is equivalent to the fields produced by the actual radiation source [22]. Applying the boundary conditions of a

The research was carried out at the expense of Russian Science Foundation grant 23-79-10165, https://rscf.ru/project/23-79-10165/.

perfect electric conductor (PEC) reduces the number of dipole moments, which simplifies the problem. This reduction is justified because the dimensions of the radiation source are significantly smaller than the ground plane, which can be treated as a PEC.

According to image theory [23], radiation from the electric P_x, P_y and magnetic M_z dipole moments is almost entirely suppressed due to interaction with their reflected copies, as the latter are oriented oppositely to the originals. In contrast, the P_z, M_x, and M_y dipole moments remain because their images reinforce the original field amplitude by being oriented in the same direction [21]. Consequently, calculating dipole moments near a PEC plane only requires measuring the tangential magnetic field components of the DUT.

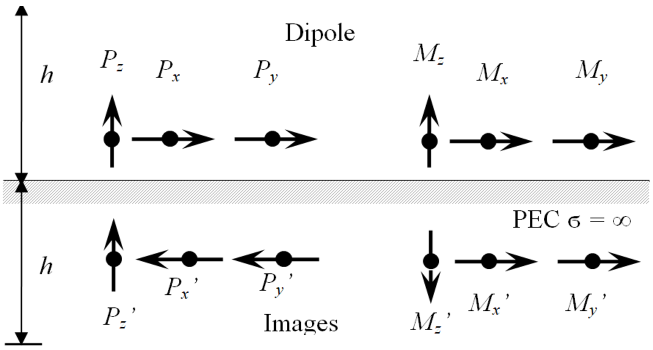

Fig. 1. Electric and magnetic dipoles and their images

The electric and magnetic dipole moment vectors are defined as:

$$\mathbf{P} = \int_v \mathbf{J}(\mathbf{r}')dv', \qquad \mathbf{M} = \frac{1}{2}\int_v \mathbf{r} \times \mathbf{J}(\mathbf{r}')dv', \tag{1}$$

where $\mathbf{J}$ is the current density distributed over the volume v', and $\mathbf{r}'$ is the vector defining the location of the observation point.

The magnetic (M_x, M_y) and electric (P_z) dipole moments were calculated from the tangential magnetic field components (H_x, H_y) measured in the near-field of the DUT as follows:

$$\begin{pmatrix} H_x \\ H_y \end{pmatrix} = \mathbf{T}\begin{pmatrix} P_z \\ M_y \\ M_x \end{pmatrix}, \tag{2}$$

where $\mathbf{T}$ is the matrix relating the dipole moments to the measured magnetic field intensity.

Each element of matrix $\mathbf{T}$ describes the contribution of a specific dipole moment to a particular field component at a local measurement point. The components of matrix $\mathbf{T}$ were determined as follows [7]:

$$\mathbf{T} = \begin{pmatrix} T_{H_xP_z} & T_{H_xM_x} & T_{H_xM_y} \\ T_{H_yP_z} & T_{H_yM_x} & T_{H_yM_y} \end{pmatrix}. \tag{3}$$

B. *Setup for Measuring Near-Field Radiated Emission Levels*

Based on the aforementioned calculations of dipole moment and boundary conditions, we developed a methodology for converting the measured near-field radiated emission levels into equivalent radiation sources. This methodology relies on measuring tangential magnetic field components and calculating dipole moments from them. To measure the radiated emission levels from the DUT, we used a setup consisting of a positioning system, a measurement receiver, control and data acquisition systems, and a probe (Fig. 2). Initially, the probe sequentially moved to points within the measurement area to record the field strength. The distance between the probe and the DUT must satisfy the near-field radiation condition. Fig. 3 illustrates the PCB layout and the measurement area consisting of measurement points. Accurate source localization requires an optimal spatial step, which is limited by the positioning capabilities of the system, while avoiding an excessive number of measurement points. The distance from the DUT to the measurement area (h) must be sufficient to encompass all radiation sources and must exceed the height of the tallest PCB component. The measured field amplitudes and probe coordinates were recorded in the data acquisition system. Using these measured values, we calculated the P_z, M_x and M_y dipole moments.

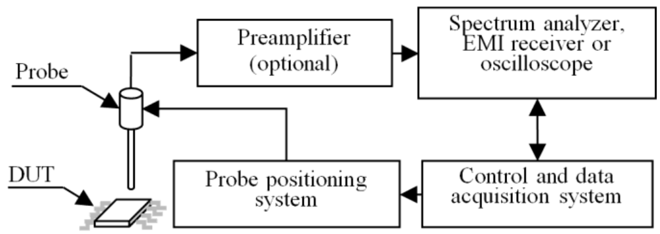

Fig. 2. Set-up for measuring DUT radiated emissions

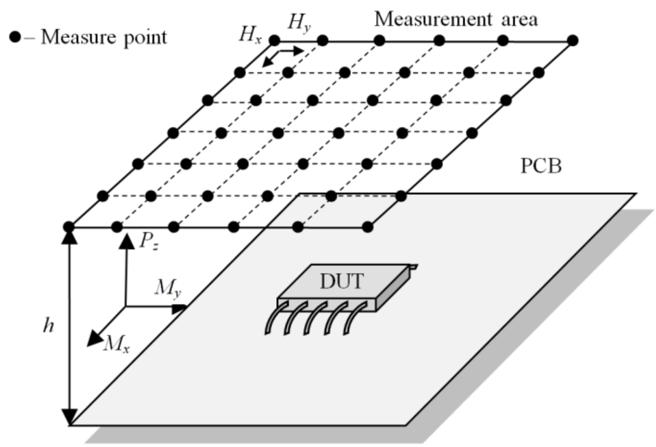

Fig. 3. PCB and its radiation model using three equivalent dipole moments

C. *Solving the Inverse Problem for Dipole Moment Calculation*

Calculating dipole moments from the measured near-field magnetic field requires solving (2). To address this inverse problem, we applied the least squares method. Furthermore, the measurement results were pre-normalized as follows:

$$F_n = \begin{pmatrix} H_x / H_{\max} \\ H_y / H_{\max} \end{pmatrix}, \tag{4}$$

where H_{max} is the maximum field intensity value among the H_y and H_x components. We also normalized the sought equivalent dipole moments as:

$$\mathbf{X}_k = \begin{pmatrix} P_z \\ k_0 M_x \\ k_0 M_y \end{pmatrix}. \quad (5)$$

This approach improved the conditioning of matrix **T** and increased the accuracy of the inverse problem solution.

$$\mathbf{F}_n = \mathbf{T}_{nk}\mathbf{X}_k, \quad (6)$$

where $\mathbf{T}_{nk}$ is defined as:

$$\mathbf{T}_{nk} = \begin{pmatrix} \frac{T_{H_x P_z}}{H_{max}} & \frac{T_{H_x M_x}}{H_{max} k_0} & \frac{T_{H_x M_y}}{H_{max} k_0} \\ \frac{T_{H_y P_z}}{H_{max}} & \frac{T_{H_y M_x}}{H_{max} k_0} & \frac{T_{H_y M_y}}{H_{max} k_0} \end{pmatrix}. \quad (7)$$

Several factors significantly affect the inverse problem results, including measurement noise, numerical errors, and the potential non-physicality of the calculated moments. The latter occurs when a solution is numerically correct but does not reflect the actual field distribution. To mitigate these issues, we employed a regularization method, specifically, truncated singular value decomposition (TSVD), to represent matrix $\mathbf{T}_{nk}$ [21].

$$\mathbf{T}_{nk} = \mathbf{USV}', \quad (8)$$

where **V** and **U** are unitary matrices of sizes $n \times n$ and $k \times k$, respectively. This approach yields the solution for the P_z, M_x and M_y dipole moments at each spatial point.

III. Results

To validate the methodology for converting measured radiated emissions into equivalent dipole sources, we developed a measurement setup (Fig. 4). The magnetic field intensity amplitude was measured using a loop probe and a Rohde&Schwarz ESPR 7 EMI test receiver.

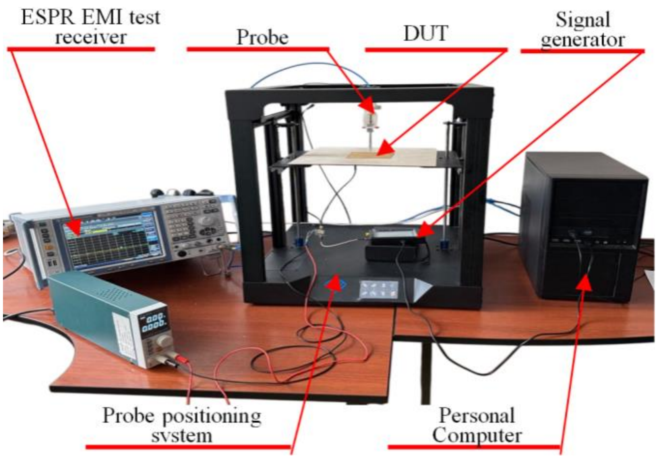

Fig. 4. Radiated emission measurement setup

The following DUTs were selected for validation: a microstrip transmission line (MSL) (Fig. 5a), a meander line (ML) (Fig. 5b), and an STM32F103C8T6 microcontroller (MCU) (Fig. 5c). The MSL was chosen as it represents a fundamental structure widely used in PCB designs. The ML allows investigating radiation non-uniformities at conductor bends, while the MCU was selected as a ubiquitous component in modern electronic systems.

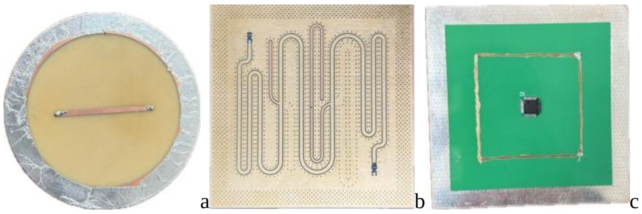

Fig. 5. Test objects for the study: (*a*) MSL, (*b*) ML, and (*c*) MCU

The radiated emission levels from the MSL and the ML were measured at 100 MHz. At this frequency, the DUT dimensions remain electrically small, which is a necessary condition for their accurate representation as a set of elementary dipoles. Moreover, the wavelength at this frequency ensures near-field radiation conditions. During the experiment, a matched load was connected to one end of the transmission line, and a 0 dBm signal was applied to the other. To assess the MCU radiation, we developed a test task that initializes the MCU at an 8 MHz clock frequency with active I/O port toggling.

Subsequently, the P_z, M_x and M_y dipole moments were calculated using the least squares method and truncated singular value decomposition (TSVD). To validate the results, the H_x and H_y magnetic field intensities were reconstructed from the calculated dipole moments. Fig. 6 shows the measured H_x and H_y magnetic field components for the MSL

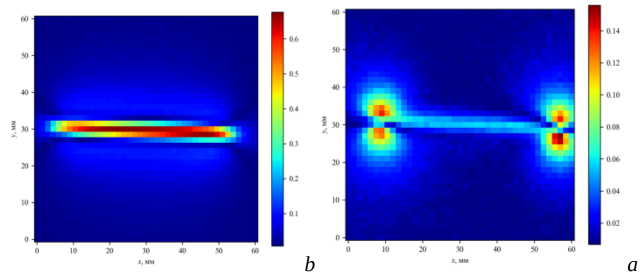

Fig. 6. Measured H_x (*a*) and H_y (*b*) field patterns of the MSL

To validate the measurements, we performed a Finite-Difference Time-Domain simulation of the MSL. The simulation results, shown in Figs. 7(a) and 7(b), indicate that the radiation patterns and peak intensity levels for the H_x component correlate well with the experimental data. Discrepancies in the H_y component may arise from numerical modeling limitations. For a more detailed visual comparison, Figs. 7(c) and 7(d) illustrate the field distributions along a line passing through the center of the *y*-axis.

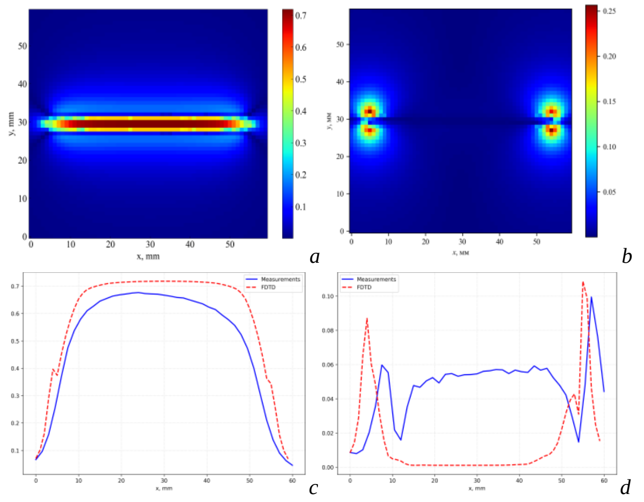

Fig. 7. Magnetic field patterns for the MSL: simulated H_x (*a*) and simulated H_y (*b*); and distribution differences along the x-axis centerline for H_x (*c*) and H_y (*d*).

Based on the measured H_x and H_y components, we calculated the equivalent dipole moments P_z, M_x, and M_y (Fig. 8). Then, we used them to reconstruct the magnetic field distributions (Fig. 9). Similar studies were conducted for the ML (Fig. 10–12) and the MCU (Fig. 13–15).

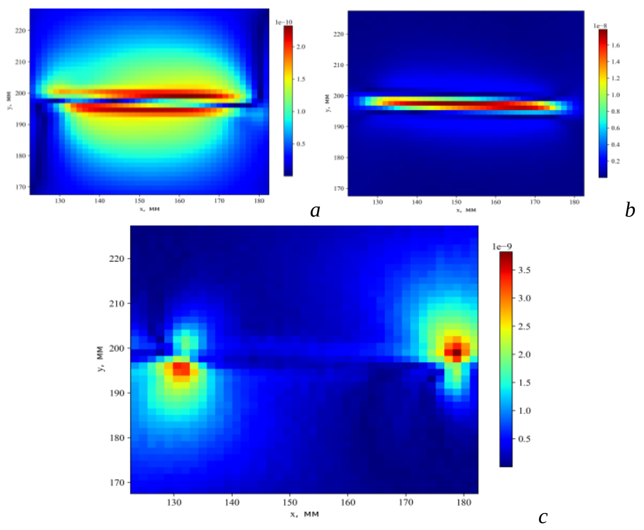

Fig. 8. Calculated dipole moments P_z (*a*), M_x (*b*), and M_y (*c*) for the MSL

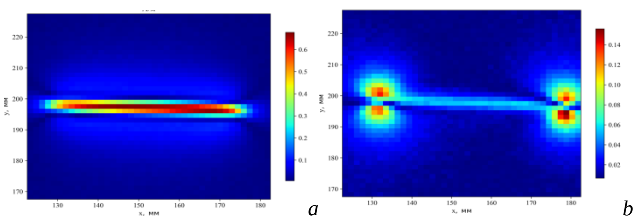

Fig. 9. H_x (*a*) and H_y (*b*) field distributions calculated from the dipole moments for the MSL

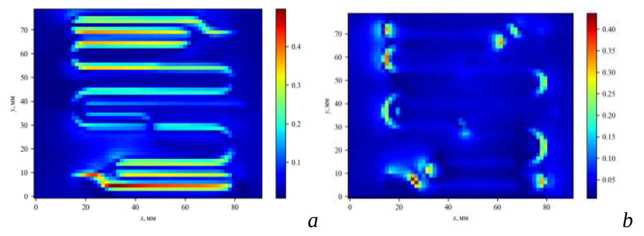

Fig. 10. Measured H_x (*a*) and H_y (*b*) field distributions for the ML

The differences in the field distributions of the ML (Fig. 10) could have been caused by the structure geometry. In an ML, the current changes direction at each bend, forming a complex interference pattern. The H_x component (Fig. 10*a*) exhibits maxima along straight conductor sections because the magnetic field generated by the current was oriented perpendicular to the conductor. Conversely, the H_y component (Fig. 10*b*) reflects the highest current density at the meander corners, where abrupt changes in current direction generated perpendicular field components that were enhanced by interference between adjacent sections.

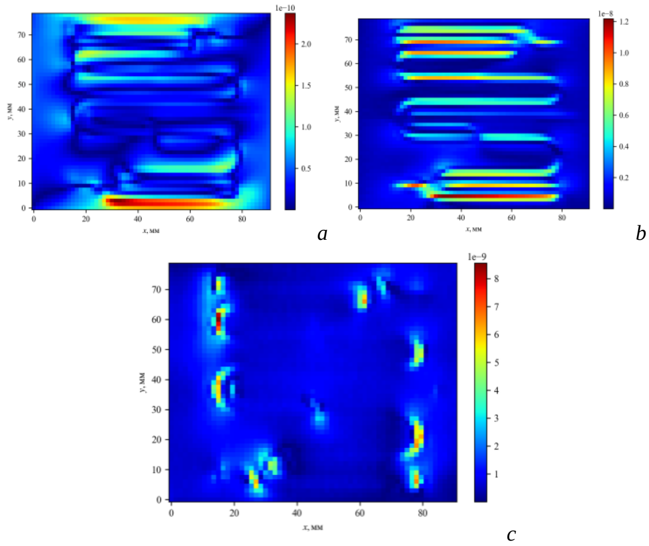

Fig. 11. Calculated dipole moments P_z (*a*), M_x (*b*), and M_y (*c*) of the ML

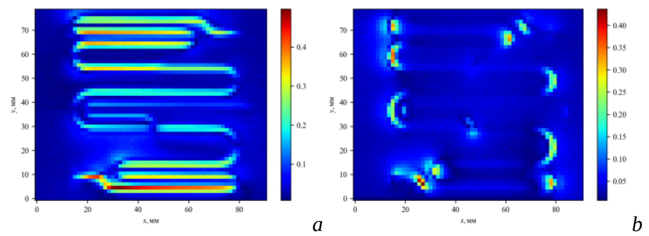

Fig. 12. H_x (*a*) and H_y (*b*) field distributions calculated from the dipole moments for the ML

Similar procedures were employed to validate the MCU (Figs. 13–15). The results show that the measured and reconstructed H_x and H_y field intensity amplitudes are in good agreement.

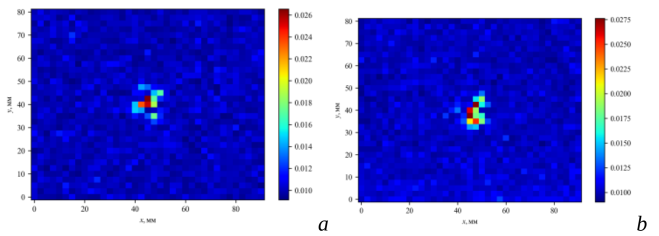

Fig. 13. Measured H_x (*a*) and H_y (*b*) field distributions for the MCU.

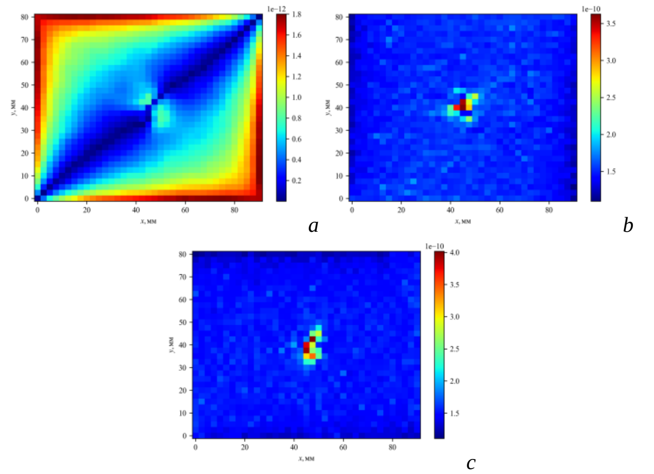

Fig. 14. Calculated dipole moments P_z (*a*), M_x (*b*), and M_y (*c*) for the MCU

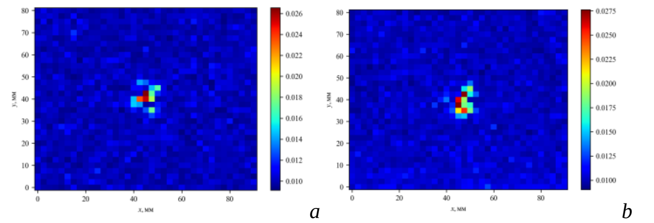

Fig. 15. H_x (*a*) and H_y (*b*) field distributions calculated from the dipole moments for the MCU

For all investigated structures (MSL, ML, and MCU), a high correlation exists between the measured magnetic field amplitudes and those reconstructed from the dipole moments (Table I).

TABLE I. ABSOLUTE DEVIATION BETWEEN MEASURED AND CALCULATED H_X AND H_Y FIELDS

DUT	H_x	H_y
MSL	6.9×10^{-15}	2.8×10^{-14}
ML	9.2×10^{-15}	1.9×10^{-14}
MCU	7.6×10^{-15}	1.0×10^{-14}

IV. CONLCUSION

In this paper, we presented a methodology for transforming near-field measurements into equivalent radiation sources by extracting electric and magnetic dipole moments from the measured magnetic field intensity. We also describe the experimental setup used for magnetic field measurements, and to validate the approach, we measured the radiated emission levels produced by an MSL, a ML, and an MCU.

The experimental results for all three test structures demonstrate high correlation between the measured and reconstructed magnetic field components, confirming both the measurement accuracy and the robustness of the dipole approximation. The maximum average deviation between the measured and calculated field amplitudes remained as low as 28 f A/m, with total field reconstruction errors staying below 1% in all cases. Such consistency across diverse geometries from simple transmission lines to complex integrated circuits validates the universal applicability of the proposed methodology for PCB-level EMC analysis.

The proposed approach enables the conversion of raw near-field scan data into compact, computationally efficient mathematical models. These equivalent sources can be seamlessly integrated into professional CAD environments for system-level simulation and far-field radiation prediction. Future research will focus on extending this methodology to higher frequency ranges and more complex multi-layer PCB layouts.

REFERENCES

[1] Integrated Circuits – Measurement of Electromagnetic Emissions, 150 kHz to 1 GHz – Part 1: General Conditions and Definitions, IEC 61967-1 Ed. 1.0, 56 p., 2002. ISBN: 978-2-8322-6986-2

[2] Integrated Circuits – Measurement of Electromagnetic Emissions, 150 kHz to 1 GHz – Part 2: Measurement of Radiated Emissions, TEM-cell Method, IEC 61967-2 Ed. 1.0, 52 p., 2005. ISBN: 2831881684

[3] Integrated Circuits – Measurement of Electromagnetic Emissions, 150 kHz to 1 GHz – Part 3: Measurement of Radiated Emissions, Surface Scan Method (10 kHz to 3 GHz), IEC 61967-3 TS Ed. 2.0, 78 p., 2012. ISBN: 9782832218099

[4] F. de Daran, J. Chollet-Ricard, F. Lafon, and O. Maurice, "Prediction of the field radiated at one meter from PCB's and microprocessors from near EM field cartography," in Proc. 2003 IEEE Int. Symp. Electromagn. Compat. (EMC'03), vol. 1, pp. 479-482, 2003. doi: 10.1109/ICSMC2.2003.1428296.

[5] P. Wilson, "On correlating TEM cell and OATS emission measurements," IEEE Trans. Electromagn. Compat., vol. 37, no. 1, pp. 1-16, 1995, doi: 10.1109/15.350235.

[6] Z. Yu, J. A. Mix, S. Sajuyigbe, K.P. Slattery, R.E. DuBroff, and J. Fan, "An improved dipole-moment model based on near-field scanning for characterizing near-field coupling and far-field radiation from an IC," IEEE Trans. Electromagn. Compat., vol. 55, no. 1, pp. 97-108, Feb. 2013, doi: 10.1109/TEMC.2012.2207726.

[7] Q. Huang, F. Zhang, T. Enomoto, J. Maeshima, B. Bae, J.L. Drewniak, and J. Fan, "Physics-based dipole moment source reconstruction for RFI on a practical cellphone," IEEE Trans. Electromagn. Compat., vol. 59, no. 6, pp. 1693-1700, Dec. 2017, doi: 10.1109/TEMC.2017.2705641.

[8] C. Wu, Y. Wang, L. Li, and J. Pan, "Estimating the near field coupling from SMPS circuits to a nearby antenna using dipole moments," in Proc. 2016 IEEE Int. Symp. Electromagn. Compat. (EMC), 2016, pp. 353-357, doi: 10.1109/ISEMC.2016.7571672.

[9] Q. Huang and J. Fan, "Machine learning based source reconstruction for RF desense," IEEE Trans. Electromagn. Compat., vol. 60, no. 6, pp. 1640-1647, Dec. 2018, doi: 10.1109/TEMC.2018.2797132.

[10] H.H. Chuang, G.H. Li, E. Song, H.H. Park, H.B. Park, K.P. Slattery, and J. Fan, "A magnetic-field resonant probe with enhanced sensitivity for RF interference applications," IEEE Trans. Electromagn. Compat., vol. 55, no. 6, pp. 991-998, Dec. 2013, doi: 10.1109/TEMC.2013.2248011.

[11] G. Li, K. Itou, Y. Katou, N. Mukai, M. Hirao, H.H. Chuang, and J. Fan, "A resonant E-field probe for RFI measurements," IEEE Trans. Electromagn. Compat., vol. 56, no. 6, pp. 1719-1722, Dec. 2014, doi: 10.1109/TEMC.2014.2333010.

[12] H. Fan and F. Schlagenhaufer, "Near field-far field conversion based on genetic algorithm for predicting radiation from PCBs," in Proc. 2007 IEEE Int. Symp. Electromagn. Compat., pp. 1-6, 2007. doi: 10.1109/ISEMC.2007.154.

[13] J.R. Regue, M. Ribó, J. Gomila, A. Pérez, and P. Rodríguez-Cepeda, "Modeling of radiating equipment by distributed dipoles using metaheuristic methods," in Proc. 2005 Int. Symp. Electromagn. Compat. (EMC 2005), vol. 2, pp. 596-601, 2005. doi: 10.1109/ISEMC.2005.1513584.

[14] Y. Vives-Gilabert, C. Arcambal, A. Louis, and P. Eudeline, "Modeling magnetic emissions combining image processing and an

optimization algorithm," IEEE Trans. Electromagn. Compat., vol. 51, no. 4, pp. 909-918, Nov. 2009, doi: 10.1109/TEMC.2009.2032171.

[15] Y.A. López, F.L.H. Andrés, M.R. Pino, and T.K. Sarkar, "An improved super-resolution source reconstruction method," IEEE Trans. Instrum. Meas., vol. 58, no. 11, pp. 3855-3866, Nov. 2009, doi: 10.1109/TIM.2009.2020847.

[16] Q. Huang, L. Li, X. Yan, B. Bae, J.L. Drewniak, and J. Fan, "MoM based current reconstruction using near-field scanning," in Proc. 2017 IEEE Int. Symp. Electromagn. Compat. & Signal/Power Integrity (EMCSI), pp. 549-554, 2017. doi: 10.1109/ISEMC.2017.8077930.

[17] Q. Huang, L. Li, X. Yan, B. Bae, J.L. Drewniak, and J. Fan, "MoM-based ground current reconstruction in RFI application," IEEE Trans. Electromagn. Compat., vol. 60, no. 4, pp. 1121-1128, Aug. 2018, doi: 10.1109/TEMC.2018.2791539.

[18] High-performance 3D EM analysis software package. [Online]. Available: https://www.3ds.com/products/simulia/cst-studio-suite.

[19] 3D Electromagnetic Field Simulator for RF and Wireless Design, [Online]. Available: https://www.ansys.com/products/electronics/ansys-hfss.

[20] C. Leseigneur, O. Kröning, P.F. López, D. Baudry, S. Bendhia, and B. Mazari, "Analysis of transmission line coupling with a near-field excitation," presented at the 7th Int. Workshop Electromagn. Compat. Integr. Circuits (EMC Compo 09), Toulouse, France, pp. 1-5, Nov. 2009.

[21] J.D. Jackson, Classical Electrodynamics, 3rd ed. New York, NY, USA: John Wiley & Sons, pp. 60-120, 1999. ISBN: 978-3-031-05099-2.

[22] C.S. Helrich, The Classical Theory of Fields: Electromagnetism. Berlin, Germany: Springer Science & Business Media, pp. 15-45, 2012. ISBN: 978-3-642-23205-3

[23] R. Ramesan and D. Madathil, "Modeling of radiation source using an equivalent dipole moment model," Prog. Electromagn. Res. B, vol. 89, pp. 157-175, 2020, doi:10.2528/PIERB20102103